# Characterization of SiaA, a Streptococcal Heme-Binding Protein Associated with a Heme ABC Transport System†

Brian R. Sook,‡ Darci R. Block,§ Suganya Sumithran,|| Griselle E. Montañez,⊥ Kenton R. Rodgers,§ John H. Dawson,|| Zehava Eichenbaum,⊥ and Dabney W. Dixon*,‡

*Department of Chemistry, Georgia State University, Atlanta, Georgia 30302-4098, Department of Chemistry, Biochemistry, and Molecular Biology, North Dakota State University, Fargo, North Dakota 58105-5516, Department of Chemistry and Biochemistry, University of South Carolina, Columbia, South Carolina 29208, and Department of Biology, Georgia State University, Atlanta, Georgia 30303*

*Received August 9, 2007; Revised Manuscript Received November 29, 2007*

ABSTRACT: Many pathogenic bacteria require heme and obtain it from their environment. Heme transverses the cytoplasmic membrane via an ATP binding cassette (ABC) pathway. Although a number of heme ABC transport systems have been described in pathogenic bacteria, there is as yet little biophysical characterization of the proteins in these systems. The *sia* (*hts*) gene cluster encodes a heme ABC transporter in the Gram positive *Streptococcus pyogenes*. The lipoprotein-anchored heme binding protein (HBP) of this transporter is SiaA (HtsA). In the current study, resonance Raman (rR), magnetic circular dichroism (MCD), and nuclear magnetic resonance (NMR) spectroscopies were used to determine the coordination state and spin state of both the ferric and ferrous forms of this protein. Identifiers from these techniques suggest that the heme is six-coordinate and low-spin in both oxidation states of the protein, with methionine and histidine as axial ligands. SiaA has a p$K_a$ of 9.7 ± 0.1, attributed to deprotonation of the axial histidine. Guanidinium titration studies show that the ferric state is less stable than the ferrous state, with $\Delta G(H_2O)$ values for the oxidized and reduced proteins of 7.3 ± 0.8 and 16.0 ± 3.6 kcal mol$^{-1}$, respectively. The reductive and oxidative midpoint potentials determined via spectroelectrochemistry are 83 ± 3 and 64 ± 3 mV, respectively; the irreversibility of heme reduction suggests that redox cycling of the heme is coupled to a kinetically sluggish change in structure or conformation. The biophysical characterization described herein will significantly advance our understanding of structure−function relationships in HBP.

Many pathogenic bacteria obtain some or all of the heme required for biosynthetic and energy utilization pathways by importing heme from their host. One method of acquiring heme is via ATP-binding cassette (ABC[1]) transporters (*1*−*3*). These are composed of a heme binding protein (HBP), a membrane permease, and an ATPase. The heme is first bound by the HBP, which then transfers it to the permease component of the transporter for passage through the cell membrane (*1*). The process is driven by the hydrolysis of ATP. Although this heme uptake pathway has been investigated in a number of organisms (*4*−*6*), it is only in the last 3 years that studies have begun to assess the spectroscopic and structural details of heme binding in the HBP. It has been found that ShuT from *Shigella dysenteriae* has a single tyrosine as the axial ligand (*7*). For IsdE (*8*), the HBP from *Staphylococcus aureus* (*9*), UV−visible absorbance spectroscopy and magnetic circular dichroism data were consistent with either a His-Tyr or Met-His axial ligand set; a recent X-ray structure shows the ligands to be methionine and histidine (*10*).

*Streptococcus pyogenes*, also known as Group A streptococcus (GAS), is a pathogenic Gram positive bacterium that causes a variety of infections (*11*). A number of heme-containing sources can support in vitro growth of this organism, including hemoglobin, the haptoglobin−hemoglobin complex, myoglobin, heme−albumin, and catalase (*12*, *13*). An ABC heme transporter in this organism is encoded by the *sia* (*Streptococcal i*ron *a*cquisition) gene cluster (*14*), also known as the *hts* (*h*eme *t*ransport *S. pyogenes*) (*15*) gene cluster. In this ABC transport system, the heme-binding lipoprotein is SiaA; it is associated with SiaB and SiaC, the membrane permease and ATPase, respectively. The proximal heme donor to SiaA in this Gram positive bacteria may be Shp, a cell surface protein encoded by the gene upstream of SiaA in the cluster. Shp can acquire heme from hemoglobin and donate it to SiaA (*16*, *17*). ESR

† This work was supported by National Institutes of Health Grants AI057877 (to Z.E.), AI072719-01 (to K.R.R.), and GM 26730 (to J.D.) and the Molecular Basis of Disease Program at Georgia State University (D.W.D.).

* To whom correspondence should be addressed. Phone: 404-413-5508. Fax: 404-413-5505. E-mail: ddixon@gsu.edu.

‡ Department of Chemistry, Georgia State University.

§ North Dakota State University.

|| University of South Carolina.

⊥ Department of Biology, Georgia State University.

[1] Abbreviations: ABC, ATP-binding cassette transporter; CCD, charge-coupled device; EK, enterokinase; CDH, cellobiose dehydrogenase; *Ec*cyt $b_{562}$, cytochrome $b_{562}$ from *E. coli*; *Ec*Dos, direct oxygen sensor from *E. coli*; ESI, electrospray ionization mass spectrometry; ESR, electron spin resonance; GdnCl, guanidine HCl; HBP, heme binding protein; LMCT, ligand to metal charge transfer; MALDI, matrix-assisted laser desorption/ionization mass spectrometry; MCD, magnetic circular dichroism; NMR, nuclear magnetic resonance; rR, resonance Raman spectroscopy; SiaA, streptococcal iron acquisition protein A; 6c LS, six-coordinate low spin.

10.1021/bi701604y CCC: $40.75 
Published on Web 02/02/2008

studies on SiaA are consistent with a bisligated heme center (*17*), but the axial ligands have not yet been reported.

Herein we report that the heme in SiaA has methionine and histidine as axial ligands, as shown by evidence from resonance Raman spectroscopy (rR), magnetic circular dichroism (MCD), and nuclear magnetic resonance (NMR) spectroscopies. The reduction potential of the protein has been measured by spectroelectrochemistry. The effect of the oxidation state on the stability of the protein has been evaluated by conformational stability studies using guanidine HCl (GdnCl) as a denaturant.

## MATERIALS AND METHODS

*Expression and Purification of SiaA*. SiaA was expressed and purified from Top10/pSiaA-His cells as previously described (*14*) with small modifications. The plasmid, pSiaA-His, expresses recombinant SiaA with an N-terminal fusion to a six-His-Xpress epitope from the arabinose-regulated promoter, PBAD (*18*). An enterokinase (EK) site downstream of the Xpress epitope facilitates the removal of the tag from the SiaA protein after purification, leaving eight residues (DRWGSELE) that are not part of the SiaA sequence (which begins with VNQHPKTA, omitting the native N-terminal signal sequence). The six-histidine tag was removed for some experiments.

SiaA expression was induced with 0.02% arabinose for 4 h. The cell pellet was broken twice with a French press in 45 mL of buffer containing 20 mM Tris-HCl (pH 8.0), 100 mM NaCl, 0.1% Triton X-100, 10% v/v glycerol, and four tablets of protease inhibitor (Roche Complete Mini, EDTA-free). The solution was cooled on ice between lysing cycles. It was then centrifuged for 20 min at 35,000 × *g*, and the supernatant was syringe-filtered with a 0.45 $\mu$m filter (surfactant-free cellulose acetate membrane, Nalgene). All of the following purification steps were conducted at 4 °C using a fast protein liquid chromatography instrument (FPLC, Amersham BioSciences), and all buffer solutions were pH 8.0 unless specified otherwise. The sample was loaded onto a nickel chelating column (5 mL HiTrap Chelating HP column, Amersham BioSciences) equilibrated with binding buffer (50 mM potassium phosphate, 250 mM NaCl, and 10% v/v glycerol). Unbound material was washed out with 5 column volumes of binding buffer. SiaA was eluted with 25 column volumes of buffer containing 50 mM potassium phosphate, 250 mM NaCl, 10% v/v glycerol, and 0.5 M imidazole applied via a linear gradient (0−100% imidazole). Fractions were collected, and their SiaA content was qualitatively evaluated by SDS−PAGE. Fractions containing SiaA were pooled, and imidazole and salts were removed by centrifugal filtration (Amicon Ultra-15, 5 kDa molecular weight cutoff, Millipore) using a buffer of 20 mM Tris-HCl and 10% v/v glycerol (designated as Buffer A).

Total protein concentration was measured using the modified Lowry assay (Pierce Biotechnology, Inc.) with a Varian Cary 50 Bio spectrophotometer. Enterokinase cleavage of the N-terminal six-histidine tag was performed in a solution containing 0.1 units of EKMax (Invitrogen Corporation), 3 $\mu$L EKMax buffer, and 20 $\mu$g of protein, diluted with water to a final volume of 30 $\mu$L. (One unit of enterokinase is defined as the amount of enzyme that will cleave 20 $\mu$g of thioredoxin−chloramphenicol acetyl transferase fusion protein to 90% completion in 16 h at 37 °C in 50 mM Tris-HCl, 1 mM $CaCl_2$, and 0.1% Tween-20.) The solution was incubated overnight (approximately 16 h) at 4 °C followed by incubation at room temperature (about 22 °C) for approximately 12 h. SDS−PAGE was used to verify cleavage. SiaA was equilibrated with Buffer A using a centrifugation filter as described above. The protein solution was loaded onto a strong anion-exchange column (5 mL HiTrap Q HP, Amersham BioSciences) equilibrated with Buffer A. Unbound protein was washed out with 5 column volumes of Buffer A and eluted with 25 column volumes of Buffer A containing 1 M NaCl applied via a linear gradient (0−100% NaCl). Fractions were collected, and purity was demonstrated by overloading an SDS−PAGE gel with sample. Fractions showing no contaminants were pooled, equilibrated with Buffer A using a centrifugation filter as described above, and stored at −80 °C.

*Mass Spectrometry*. Matrix-assisted laser desorption/ionization mass spectrometry (MALDI) was performed using an ABI Voyager DE-Pro (Applied Biosystems) MALDI reflectron time-of-flight spectrometer in positive ion mode. The sinipinic acid matrix was prepared in 30:70 acetonitrile/water and 0.1% trifluoroacetic acid. The sample solution was mixed with the matrix solution in a 1:1 ratio and the resulting solution spotted onto the MALDI target plate. Electrospray ionization mass spectrometry (ESI) was performed using a Micromass Q-TOF Micro mass spectrometer in positive mode. Samples were prepared in a solution containing 50:50 acetonitrile/water and 0.1% formic acid. The capillary voltage was 3.0 kV, and the flow rate was 5 $\mu$L/min. Deconvolution of the charge state distribution was performed with the MaxEnt program included with the MassLynx software. Throughout the text, peaks are rounded to the nearest Dalton.

*Nuclear Magnetic Resonance*. Protein samples were prepared by equilibration with deuterated 50 mM potassium phosphate, adjusted to pD 7.4. The sample was deoxygenated with nitrogen in a screw cap septum NMR tube (Wilmad), and a solution of deoxygenated buffered sodium dithionite (approximately 10-fold excess of reducing agent) was injected into the NMR tube to reduce the protein. $^1$H NMR spectra of the reduced protein were recorded on a 500 MHz Varian Unity+ instrument at 25 °C using water suppression. Proton chemical shifts were referenced to water at 4.77 ppm.

The NMR of the heme methyl resonances of the protein in the paramagnetic region (20 to 45 ppm) was unaffected by the presence or absence of the six-His-Xpress epitope, indicating that the histidines in the His tag do not interact with any heme in solution and that the presence of the N-terminal sequence does not alter the heme binding site. Experiments were therefore performed with both the full construct and the enterokinase-cleaved form, as indicated in the description of each experiment.

*Resonance Raman Spectroscopy and pH Effects*. Resonance Raman spectra of the enterokinase-cleaved form of SiaA were excited using 413.1 nm emission from a $Kr^+$ laser. Raman scattered light was collected with *f*1 efficiency and *f* matched to an *f*4.5 0.6-m spectrograph equipped with a liquid nitrogen-cooled CCD detector. The entrance slit was set to 15 $\mu$m for all measurements. The excitation laser beam was focused to a line on the sample and its power adjusted to 5−12 mW. All samples were spun at ~20 Hz to minimize

laser-induced degradation of the protein samples. The spectra were calibrated using Raman bands from methylene bromide and toluene in the low-frequency regions and from toluene and DMF in the high-frequency regions. The resonance Raman samples used to investigate the effects of pH were prepared by diluting 20 $\mu$L of 100 $\mu$M SiaA (*17*) into 100 $\mu$L of 20 mM buffers of MES at pH 5.2 and 6.3, MOPS at pH 7.1, Tris-HCl at pH 8.0, CHES at pH 9.1, and CAPS at pH 9.9, 11.1, and 12.0. Ferrous SiaA samples were prepared by equilibration of the ferric protein solution under a purge of water-saturated $N_2$ followed by reduction with a 10-fold excess of buffered sodium dithionite solution. UV−visible spectra were recorded before and after rR experiments to ensure that the protein was not degraded by exposure to laser radiation.

*Spectrophotometric pH Titrations.* Samples for these measurements were prepared by the method described above for rR samples. Additionally, pH effects were investigated by titrating SiaA in Tris-HCl buffer, CHES buffer, and CAPS buffer by the addition of 1 $\mu$L aliquots of 1 M NaOH and 1 M HCl. These titrations were carried out using different buffers and going both directions. All pH titrations were monitored between 350 and 750 nm using a scanning spectrophotometer. The wavelength axes of the spectrometer were calibrated using the bands from holmium oxide glass. The variable pH data were analyzed using a commercial global analysis software package.

*Electrochemistry*. The midpoint reduction potential of the enterokinase-cleaved form of SiaA was determined using the spectroelectrochemical method of Dutton et al. (*19*). The oxidized and reduced heme populations were monitored as a function of cell potential by UV−visible absorbance between 350 and 650 nm using a homemade spectroelectrochemical cell and a CCD-based multichannel spectrometer. The wavelength axes of the spectrometer were calibrated using the bands from holmium oxide glass. Mediator dyes (methyl viologen, benzyl viologen, anthraquinone-2-sulfonate, anthraquinone-2,6-disulfonate, 2-hydroxy-1,4-napthoquinone, indigo disulfonate, indigo trisulfonate, indigo tetrasulfonate, pyocyanin, duroquinone, 5-hydroxy-1,4-napthoquinone, 1,4-napthoquinone, phenazine methosulfate, 2,6-dimethyl benzoquinone, 2-methyl-1,4-benzoquinone, and 1,2-napthoquinone-4-sulfonate) were used to prepare a stock cocktail solution in DMSO, whose concentration was 10 mM in each dye. This solution was diluted to a final concentration of 10 $\mu$M in each dye. Reductive and oxidative titrations were performed using microliter aliquots of 0.1 M dithionite and 0.1 M ferricyanide, respectively. Cell potential was monitored using a glass electrode and pH meter in the mV mode. Establishment of equilibrium was confirmed after each dithionite addition by monitoring voltage with a strip chart recorder. The data were analyzed using a commercial global analysis software package. The fitting model was a two component system undergoing parallel redox processes. The oxidized and reduced spectra of SiaA were fixed as the initial and final species for one of the components. The other component was a composite spectrum of the mediators whose absorbance in the 350−700 nm range also changes as a function of cell potential, yielding a second composite midpoint potential.

*Magnetic Circular Dichroism Spectroscopy.* MCD spectra were recorded at 4 °C and 1.41 T on a JASCO J600 spectropolarimeter fitted with a JASCO MCD-1B electromagnet. JASCO software was used for data acquisition and manipulation as previously reported (*20*). UV−visible absorbance spectra were recorded before and after MCD measurements to check sample integrity. All spectra were obtained using quartz cuvettes with either 0.5 or 1 cm path lengths. SiaA protein samples (enterokinase-cleaved form of the protein) were studied in 20 mM Tris-HCl at pH 8.0. The cyanide and NO adducts of ferric SiaA were prepared as previously described (*21*, *22*). The ferrous species of SiaA was prepared in a sealed cuvette by first exchanging the atmosphere in the cuvette with nitrogen followed by the addition of solid sodium dithionite.

*Conformational Stability*. Protein unfolding experiments were performed on the enterokinase-cleaved form of the protein using GdnCl as the denaturant, according to standard protocols of Pace (*23*). UV−visible absorption spectrometry (Varian 50 Bio spectrophotometer, 1.5 mL quartz black-masked Supracil cuvettes (Spectracell) with 1 cm path lengths) was used to follow the unfolding process. The refractive index was used to verify GdnCl concentration (*23*), which was 8.35 M. Approximately 5−10 $\mu$M protein in 50 mM Tris-HCl at pH 7.0 was used for the titrations. Reduced protein was created by removing oxygen via nitrogen flushing for approximately 40 min, then adding 5−10 $\mu$L of an anaerobic 0.1 M sodium dithionite solution (approximately 10-fold excess of reducing agent). During the anaerobic titrations, the sample compartment of the spectrometer was kept under positive nitrogen pressure. GdnCl was titrated into the solution and allowed to equilibrate while monitoring optical absorbance at 414 and 424 nm for the oxidized and reduced samples, respectively. Equilibrium was considered to have been established when the absorbance showed no further change. All experiments were conducted at 22 °C. The unfolding curves were analyzed using the following equation (*23*):

$$y = \{(y_F + m_F[D]) + (y_U + m_U[D] \times \exp[m \times ([D] - [D]_{1/2})/RT]\}/(1 + \exp[m \times ([D] - [D]_{1/2})/RT])$$

where $y$ is the absorbance at any point along the fitted denaturation curve, $y_F$ is the absorbance of the folded state, $y_U$ is the absorbance of the unfolded state, $m$ is the slope at the midpoint, and also the dependence of the free energy of unfolding on the denaturant concentration, $m_F$ is the slope of the folded state, $m_U$ is the slope of the unfolded state, [D] is the concentration of GdnCl, $[D]_{1/2}$ is the concentration of GdnCl at the midpoint of the unfolding curve, $R$ is the gas constant, and $T$ is the temperature (Kelvin). Kaleidagraph (version 4.01, Synergy Software) was used to fit the curve on the basis of the assumption that unfolding is a two-state process. The free energy of protein unfolding in water [$\Delta G(H_2O)$] was calculated as $\Delta G(H_2O) = m[D]_{1/2}$.

## RESULTS

*Protein Purification*. The construct used in these studies has an $Asp_4$-Lys sequence, which is the cleavage recognition site for enterokinase (*24*). Various protocols were tested to find conditions that would give pure cleaved protein with a minimum amount of enterokinase. A method using 0.1 units of enterokinase per 20 $\mu$g of the affinity-purified protein

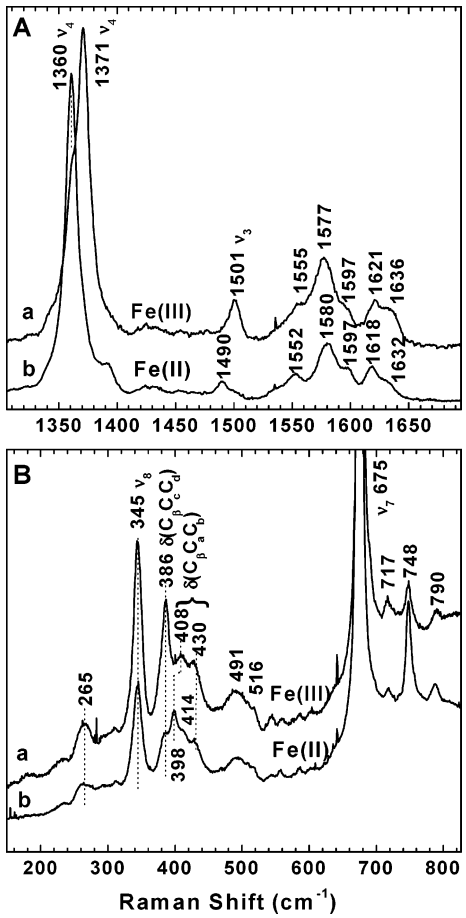


FIGURE 1: Soret-excited rR spectra of SiaA in the in-plane porphyrin stretching (A) and low frequency (B) regions. The samples are 50 $\mu$M SiaA and 10 mM Tris-HCl at pH 8.0. Spectra correspond to ferric (a) and ferrous (b) SiaA.

incubated first for 16 h at 4 °C and then for 12 h at 22 °C gave good yields of cleaved protein.

ESI of the purified protein showed masses corresponding to the predicted apo and holoproteins at 32,190 and 32,803 Da, respectively. In addition, two other masses were observed at 31,919 and 32,532 Da. The two additional peaks were ascribed to the holo and apo forms of a protein that had cleaved after the arginine in the sequence (N-terminus)-DDDDKDR-$n_8$-SiaA. Such cleavage finds precedence in situations where the ionic charge of the recognition site is preserved (*24*). Other preparations of SiaA gave complete cleavage after the arginine residue in this sequence, as shown by mass spectrometry and amino acid sequencing. MALDI mass spectra of SiaA often had associated sodium ions (*25*, *26*); different preparations had different numbers of sodium ions.

*Resonance Raman and UV−Visible Absorbance Spectroscopy of Ferric and Ferrous SiaA.* Figure 1A shows the rR spectra of ferric and ferrous SiaA from 1350 to 1650 cm$^{-1}$. The oxidation state or $\pi^*$ electron density marker, $\nu_4$, occurs at 1371 cm$^{-1}$ in Figure 1A(a) and at 1360 cm$^{-1}$ in Figure 1A(b), indicating the presence of ferric and ferrous heme, respectively. A shoulder occurs at 1360 cm$^{-1}$ in the ferric SiaA spectrum, indicating a steady-state accumulation of ferrous heme due to photoreduction in the laser beam. The corresponding spin state marker bands, $\nu_3$, occur at 1501 and 1490 cm$^{-1}$, indicative of six-coordinate and low-spin (6c LS)

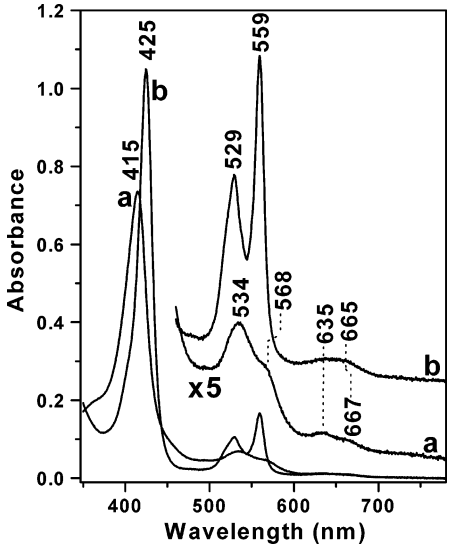


FIGURE 2: UV−visible absorbance spectra of ferric (a) and ferrous (b) SiaA in 10 mM Tris-HCl at pH 8.0.

ferric and ferrous hemes, respectively. Figure 1B shows the low-frequency rR spectra of ferric and ferrous SiaA. The rR spectra of cellobiose dehydrogenase (CDH) (*27*) and *Ec*Dos, a heme-based sensor from *E. coli* (*28*), which both contain a *b*-type heme and the Met-His axial ligand set, bear a striking resemblance to that of SiaA. The ferrous state of the protein did not bind CO(g), indicative of a highly stable and/or deeply buried 6c heme (*27*, *29*). These similarities are consistent with SiaA having an axial ligand set comparable to CDH and *Ec*Dos.

Figure 2 shows the UV−visible absorbance spectra of ferric and ferrous SiaA. Both spectra are consistent with their respective rR spectra, indicating LS hemes. Moreover, the low-intensity bands to the red of the Q bands are consistent with a S → Fe LMCT transition, indicative of an axial Met ligand (*27*, *28*, *30*).

*pH Dependence of the Resonance Raman and UV−Visible Spectra*. Figure 3A and B shows the rR spectra as a function of pH from 1350 to 1650 cm$^{-1}$ and from 300 to 800 cm$^{-1}$, respectively. The spectra reveal little sensitivity to pH in these regions of the spectrum. Whereas the low-frequency spectrum in Figure 3B shows no pH-dependent bands, Figure 3A reveals small shifts in the core size marker bands, $\nu_4$, $\nu_2$, and $\nu_{37}$, to higher frequencies with increasing pH. These spectral trends report a change in the axial ligand field.

Consistent with trends in the high-frequency rR spectra, slight variations are also observed in the UV−visible spectra as a function of pH (Figure 4A). The Soret maximum shifts 3 nm to the red as the pH is increased from 5.2 to 12.0, giving rise to the pH dependence of $A_{414}$ shown in the inset of Figure 4A. Also, the Q-band maxima and the S → Fe LMCT absorbance change systematically with pH. Noteworthy is the persistence of the LMCT band, indicating that the Met-His ligand set is maintained over the investigated pH range. Global analysis of the spectrophotometric pH titration data was based on a single protonation equilibrium model. This analysis yielded a p$K_a$ of 9.7 ± 0.1 for SiaA. Figure 4B(a) and (b) shows the calculated absorbance spectra of the acid and base forms of SiaA, and the inset shows the calculated speciation diagram in which the species curves cross at the p$K_a$. The UV−visible spectrum of SiaA and its

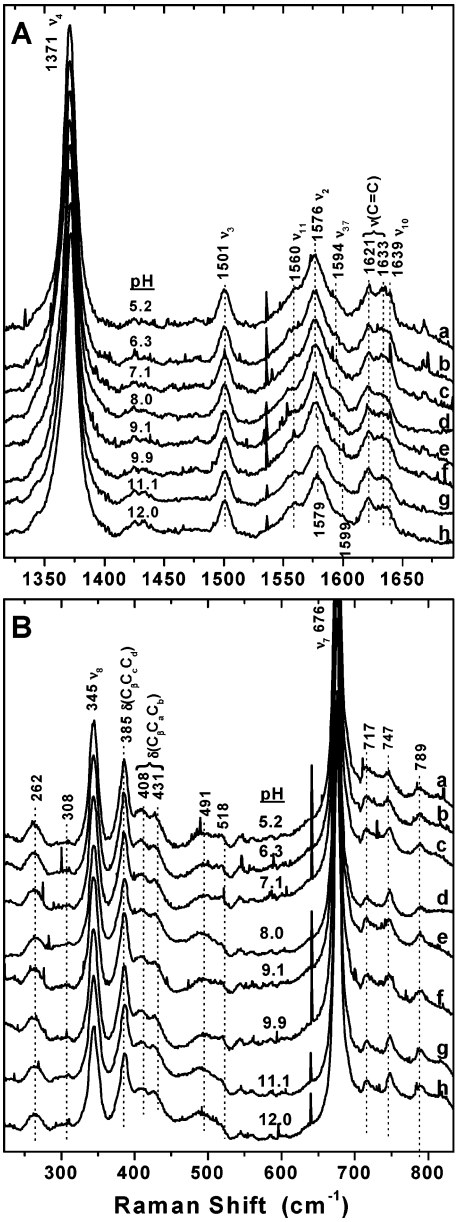


FIGURE 3: Soret-excited rR spectra of SiaA in the in-plane porphyrin stretching (A) and low frequency (B) regions. The spectra correspond to pH 5.2 (a), 6.3 (b), 7.1 (c), 8.0 (d), 9.1 (e), 9.9 (f), 11.1 (g), and 12.0 (h). The samples were prepared as described in Materials and Methods.

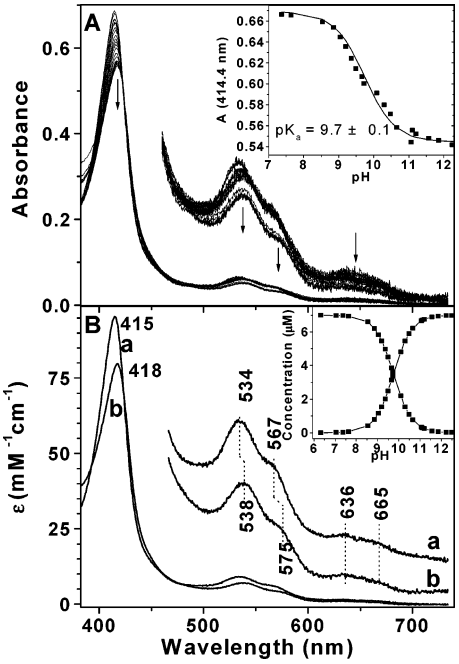


FIGURE 4: Spectrophotometric pH titration of SiaA. (A) UV−visible absorbance spectra of SiaA from pH 7.1 to 12.3. The inset shows data and fit from titration curves generated from global analysis at 414.4 nm. (B) Component spectra of the acidic (a) and basic (b) species of SiaA. The inset shows speciation of SiaA as a function of pH, calculated by global analysis.

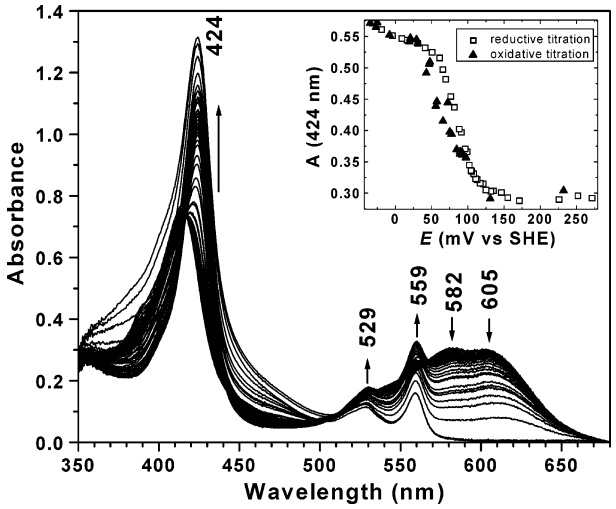


FIGURE 5: Spectrophotometric redox titration of SiaA. UV−visible absorbance spectra of SiaA titrated with dithionite. The inset shows data from oxidative and reductive titration curves at 424 nm.

pH dependence in the ferric form is comparable to that of *E. coli* cytochrome $b_{562}$ (*Ec*cyt $b_{562}$). In the pH range 4.0−6.8, *Ec*cyt $b_{562}$ has a Soret peak at 419 nm, $\beta$- and α-bands at 531 and 561 nm, respectively, and S → Fe LMCT bands at 650 and 710 nm. At pH 9.96, these bands shift to 422, 538, 568, and 630 nm, respectively (*31*). These shifts and their dependence on pH are comparable to those of SiaA, indicating similarities in their acid/base behaviors.

*Electrochemistry of SiaA.* Figure 5 shows the results from global analysis of the SiaA spectroelectrochemical titration data. The arrows on the absorbance spectra show the direction of absorbance change as the potential is decreased, and the inset shows $A_{424}$ for the reductive and oxidative titrations of SiaA. Midpoint potentials of 83 ± 3 and 69 ± 17 mV were obtained from global analysis and fitting of absorbance at 424 nm, respectively, for the reductive titration of ferric SiaA. Similar analyses of the oxidative titration yielded midpoint potentials of 64 ± 3 and 59 ± 16 mV. The irreversibility of heme reduction suggests that redox cycling of the heme is coupled to a kinetically sluggish change in structure or conformation that influences the *E*m of the Fe(III)|Fe(II) couple. The titration curves in the inset of Figure 5 exhibit a feature at low potential. It arises from absorbance changes attributable to mediator dyes and unreduced dithionite.

*Magnetic Circular Dichroism Spectroscopy.* The MCD spectra of ligand adducts of ferric SiaA are compared with parallel derivatives of myoglobin in Figure 6. The spectra of the ferric-NO (Figure 6A) and ferric-CN (Figure 6B) derivatives are quite similar to those of the analogous myoglobin adducts except for minor differences in the

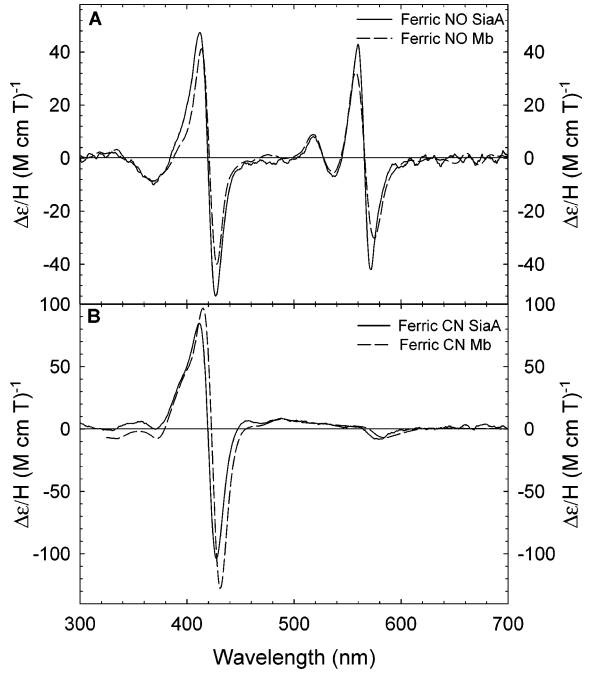


FIGURE 6: Magnetic circular dichroism spectra at 4 °C of (A) ferric-NO derivatives of SiaA in 10 mM Tris-HCl buffer at pH 8.0 (—) and myoglobin in 100 mM potassium phosphate buffer at pH 7.0 (---); (B) Ferric-CN derivatives of SiaA in 10 mM Tris-HCl buffer at pH 8.0 (—) and myoglobin in 100 mM potassium phosphate buffer at pH 7.0 (---). Ferric-NO and ferric-CN myoglobin spectra are replotted from refs *21* and *22*, respectively.

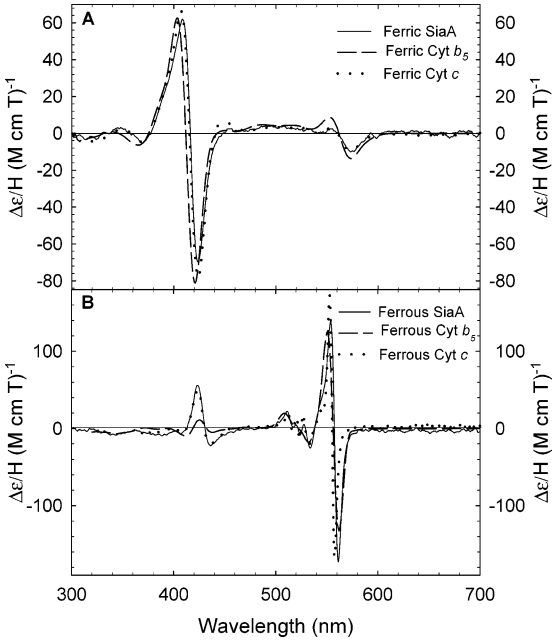


FIGURE 7: Magnetic circular dichroism spectra at 4 °C of (A) ferric SiaA in 10 mM Tris-HCl buffer at pH 8.0 (—), ferric cytochrome $b_5$ in 50 mM potassium phosphate buffer at pH 7.0 (---), and ferric cytochrome *c* in 10 mM potassium phosphate buffer at pD 7.0 (• ••); (B) ferrous SiaA in 10 mM Tris-HCl buffer at pH 8.0 (—), ferrous cytochrome $b_5$ in 50 mM potassium phosphate buffer at pH 7.0 (---), and ferrous cytochrome *c* in 9 M urea and 10 mM potassium phosphate buffer at pD 7.0 (•••). Cytochrome $b_5$ spectra are replotted from ref *37*. Cytochrome *c* spectra are from ref *34*, replotted with a shift of +9 nm (see text).

intensity of the NO derivatives and a few nanometers of spectral shift in the cyanide derivatives. This provides strong support for histidine as the fifth ligand to the heme iron of ferric SiaA. No ligation of azide or imidazole takes place with the native ferric SiaA protein even in the presence of excess ligand concentrations. CO, the ligand widely used to probe the heme environment of heme proteins, does not bind SiaA in the ferrous state.

MCD spectra of ferric and ferrous species of SiaA, cytochrome $b_5$, and cytochrome *c* are compared in Figure 7. Systems containing His-His and Met-His coordination give similar MCD spectra in the UV−visible region (*32*). Proteins with heme *c* and heme *b* with the same ligand coordination structure show similar MCD spectra, but with a 4 to 12 nm shift in the wavelength (*33*). Therefore, the spectra of both ferric and ferrous cytochrome *c* are shifted by +9 nm. Figure 7A displays the MCD spectra of ferric SiaA compared with that of cytochrome $b_5$ (His-His ligation) and cytochrome *c* (Met-His ligation). The spectrum of ferric SiaA is almost identical to that of ferric cytochrome *c* and is similar to that of cytochrome $b_5$, although the latter has a slightly higher intensity in the visible region (feature at 540−580 nm) and displays a blue shift of the Soret derivative feature by a few nanometers.

The MCD of ferrous SiaA, ferrous cytochrome *c* in urea, and cytochrome $b_5$ are plotted together in Figure 7B. Ferrous cytochrome *c* in urea has Met-His ligation, retaining the ligand set of the native protein (*34*) (spectrum not shown). However, the MCD spectral intensities are smaller for ferrous cytochrome *c* in urea, and its spectrum is more comparable to that of ferrous SiaA. All three spectra in Figure 7B are generally similar to each other in the visible region with only minor differences. However, the spectrum of ferrous SiaA displays a striking resemblance to that of ferrous cytochrome *c* in urea in the Soret region.

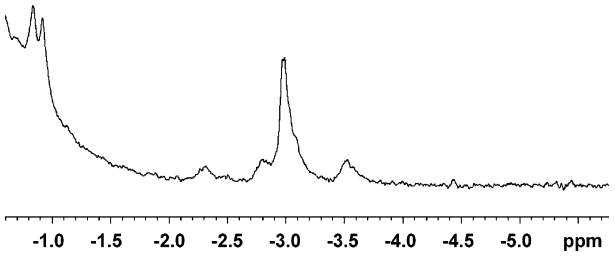


FIGURE 8: High-field region of the 500 MHz $^1$H NMR spectrum of reduced SiaA at pD 7.4 and 50 mM deuterated phosphate buffer.

*NMR Spectrum of the Reduced Protein*. The upfield region of the NMR spectrum of the ferrous form of the protein is shown in Figure 8. The three proton singlet is assigned to the $\epsilon$-Me of the methionine; this is diagnostic for a methionine axial ligand bound to the heme. Some of the other upfield single proton resonances are due to the $\beta$- and $\gamma$-protons on the methionine. Not all upfield resonances integrate to one proton because the heme binds to the protein in two orientations rotated by 180°, as seen by two sets of heme methyl groups in the ferric form of the protein (data not shown).

*Conformational Stability*. Both the ferric and ferrous forms of the protein were treated with GdnCl and the data fit with a standard two state transition model as described in Materials and Methods (Figure 9). The midpoints of the transitions occurred at 3.1 ± 0.1 and 5.0 ± 0.1 M GdnCl for the oxidized and the reduced form of the protein, respectively, indicating that the ferrous form of the protein was more stable, as expected. The conformational stabilities

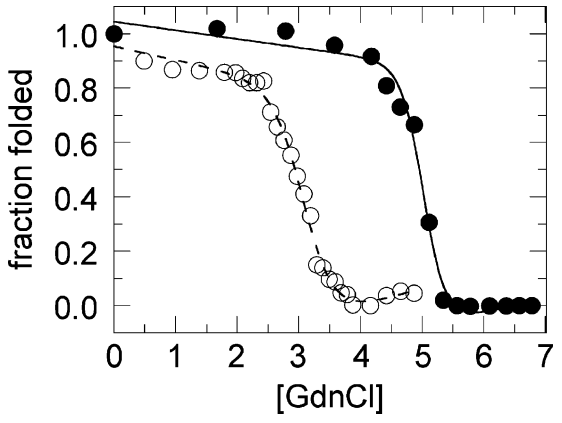


FIGURE 9: Fraction of unfolded SiaA as a function of [GdnCl] for oxidized SiaA (5 $\mu$M, ---) in 50 mM Tris-HCl at pH 7.0 and reduced SiaA (10 $\mu$M, —) in 50 mM Tris-HCl at pH 7.0. The absorbance changes were monitored at 414 nm (oxidized) and 424 nm (reduced). The lines are a fit to the equation in Materials and Methods.

[$\Delta G(H_2O)$] of the oxidized and reduced proteins were 7.3 $\pm$ 0.8 and 16.0 $\pm$ 3.6 kcal mol$^{-1}$, respectively. The *m* values, which describe the dependence of $\Delta G$ on the concentration of denaturant, were 2.4 $\pm$ 0.3 and 3.3 $\pm$ 0.6 kcal mol$^{-1}$ M$^{-1}$, respectively.

## DISCUSSION

*Met-His Axial Ligation.* A combination of the rR signatures with the MCD and NMR spectral data allows the conclusion that methionine and histidine are the axial heme ligands in SiaA. The rR data indicate that both the ferric and ferrous forms of SiaA are six-coordinate and low-spin. Although rR signatures alone do not distinguish between His-His and Met-His axial ligand sets, the spectra are consistent with Met-His axial ligation of the heme iron. Often, CO(g) is used as a probe of the heme environment, but it was found that like cellobiose dehydrogenase (CDH) (*27*, *29*), SiaA does not bind CO(g) in the ferrous state. This is typical of stable 6c LS hemes with two axial ligands.

MCD spectroscopy provides information about the coordination structure of heme−iron complexes including the determination of the oxidation state, spin state, and axial ligand identification (*35*). This is accomplished by examining the MCD spectra of the uncharacterized heme protein and several of its ligand adducts in comparison with the spectra of structurally characterized heme proteins or porphyrin model complexes. MCD spectroscopy is more useful for this approach than is UV−visible absorption spectroscopy because the MCD spectra provide better fingerprints.

Coordination of an exogenous sixth ligand to the heme iron generates a complex in which five of the six ligands are known. Comparison of the spectra of such a complex to the spectra of the structurally undefined protein with the same added exogenous ligand can then lead to the determination of the axial ligand *trans* to the exogenous ligand. In the present study, two different ligand complexes of ferric SiaA, ferric-NO and ferric-CN, were prepared and their MCD spectra overlaid with the parallel derivatives of His-ligated myoglobin (Figure 6). The MCD spectra of the two SiaA derivatives are very similar to those of the corresponding myoglobin derivatives. This provides strong support for the conclusion that SiaA has a histidine axial ligand.

The MCD spectrum of ferric SiaA is almost identical to that of ferric cytochrome *c*, which has a Met-His ligation in the given buffer conditions (*34*) (Figure 7A), allowing us to conclude that native SiaA has the same ligand pair. However, the possibility of His-His ligation cannot be ruled out as the MCD spectrum of ferric SiaA is also very similar to that of ferric cytochrome $b_5$, which has two His ligands (*36*, *37*). It is been shown by the MCD spectral studies on His-His and Met-His ferric low-spin heme systems that only NIR MCD allows one to distinguish between His-His and Met-His ligation (*32*).

To investigate the function of SiaA in heme binding and release, it is essential to also study the ligation of the iron in the ferrous state. Therefore, we have compared the MCD spectra of ferrous SiaA with those of ferrous cytochromes $b_5$ (His-His) and cytochrome *c* in urea (Met-His). Here, the spectra of ferrous SiaA match the entire spectrum of ferrous cytochrome *c* much more closely than that of ferrous cytochrome $b_5$, especially in the Soret region. We therefore conclude that SiaA is Met-His coordinated in the ferrous state.

In the NMR spectrum of a reduced Met-His heme protein, the methionine bound to the heme has a characteristic three proton singlet due to the $\epsilon$-methyl in the range from −2.9 to −3.5 ppm (*38*−*47*). At least two, and generally three or four of the $\beta$-$CH_2$ and $\gamma$-$CH_2$ protons (depending on the chirality of the methylene group and the placement of nearby residues) are also seen in the upfield region. For SiaA, the NMR of the upfield region is entirely consistent with an axial methionine ligand.

Three-dimensional sequence alignment with the related cobalamin transport protein BtuF (*48*, *49*), the iron hydroxamate-binding protein FhuD (*50*), and the enterobactin-binding protein CeuE (*51*) indicates that Met79 and His229 are the axial ligands. This hypothesis is consistent with the recent X-ray structure of the heme-binding IsdE from *S. aureus* (*10*).

*Comparison of SiaA with other b-Type Heme Proteins with the Met-His Axial Ligand Set.* There are three other *b*-type heme proteins in the protein data bank with Met-His axial ligand sets; they are *Ec*cyt $b_{562}$, a small soluble periplasmic four-helix bundle protein from *E. coli* (*52*, *53*), CDH, cellobiose dehydrogenase from the white rot fungus *Phanerochaete chrysosporium* (*27*), and *Ec*Dos, a heme-based sensor from *E. coli* (*28*). The proposed Met-His axial ligation of SiaA makes comparison of their biophysical data relevant. Both rR and UV−visible absorbance spectra clearly show that the ferric and ferrous hemes are 6c and LS. The $\nu_3$ bands for ferric and ferrous *Ec*cyt $b_{562}$ (*54*), CDH (*29*), and *Ec*Dos (*28*) have been reported at 1506 $\pm$ 1 cm$^{-1}$ and 1494 $\pm$ 1 cm$^{-1}$, respectively, indicating 6c LS heme in both oxidation states. Additionally, the reported high-frequency spectra of CDH and *Ec*Dos were recorded with Soret-excitation; these spectra have band shapes and frequencies comparable to those of SiaA. This comparison further supports SiaA having Met-His axial ligation.

The calculated p$K_a$ for SiaA of 9.7 is in the range of that reported for other heme proteins with axial histidines, attributed to deprotonation of this ligand (*47*, *55*). Reported p$K_a$ values include myoglobin (10.4) (*56*); cytochromes *c*′ (8−9.1, depending on the species) (*57*, *58*); and cytochrome $c_{550}$ from *Bacillus halodenitrificans* ($\approx$11) (*45*). While these

proteins establish a range for axial histidine deprotonation, they do not provide a direct comparison to SiaA because of differences in heme type, axial ligation, and spin state. The only p$K_a$ reported for a *b*-type heme with Met-His axial ligands of which the authors are aware is *Ec*cyt $b_{562}$ (9.0, measured by reduction potentials as a function of pH (*30*) and 8.1, measured by NMR) (*47*). The observation that the p$K_a$ for SiaA is higher than that for *Ec*cyt $b_{562}$ indicates that SiaA lacks a specific interaction of the axial histidine with a nearby residue in the protein (*30*).

*Electrochemistry*. The reduction potential of SiaA lies between 64 and 83 mV versus SHE. The range of reduction potentials for heme proteins having the Met-His axial ligand set spans approximately 400 mV (*59*, *60*). Cytochrome $b_{562}$ has a reduction potential of 167 mV (*30*, *61*, *62*). The CDH heme domains of *P. chrysosporium* and *Humicola insolens* have redox potentials of 130 and 126 mV, respectively, at pH 7.0 (*63*). Many cytochromes *c* with Met-His ligands have $E_m$ values in the 150 to 350 mV range (*64*). However, there are some with lower redox potentials, particularly from alkaliphilic variants of *Bacillus*, with $E_m$ values ranging from 50 to 100 mV (*65*). A recent study of cytochrome $c_{553}$ from *Desulfovibrio vulgaris* found an $E_m$ value of −20 mV (*66*). The reduction potential of a heme is controlled by a number of factors, including the nature of the axial ligands, attachment of the heme to the protein, solvent exposure of the heme, ionization of the propionic acids, placement of the NH groups of nearby amide linkages, interaction with buried and surface charges, and conformational change occurring upon oxidation or reduction. Gunner and co-workers have recently looked at the contributions of specific factors in determining redox potentials (*64*). They concluded that the low potential of *B. pasteurii* cytochrome $c_{553}$ (47 mV) (*67*) was due to a combination of factors, including the placement of the dipoles of the protein backbone near the heme. Overall, the redox potential of SiaA is toward the lower end of the range of Met-His proteins.

*Possible Coupling of Heme Transfer and the Oxidation State of the Protein*. SiaA has a significantly higher reduction potential than two other proteins that are also involved in heme trafficking, HasA and ShuT. HasA has tyrosine and histidine as axial ligands; it has a redox potential of −550 mV (*68*). ShuT has a tyrosine axial ligand and a reduction potential of ≤ −430 mV (*69*). The relatively high reduction potential of SiaA may indicate that heme transfer and the redox state of the heme are coupled for this protein. In solution, Shp transfers heme to SiaA with similar rate constants in the ferric and ferrous forms (*17*), indicating that either or both oxidation states might be important in the transfer process in vivo.

There are two lines of evidence that heme transfer in SiaA may be controlled in part by redox processes in the protein. First, two ORFs in the *sia* gene cluster, SiaD and SiaE, have significant homology to the CydC and CydD proteins of the *E. coli* ABC cysteine exporter. CydDC exports cysteine and glutathione in an ATP-dependent process (*70*, *71*). Cysteine export might poise the redox potential on the surface of the cell so as to favor heme uptake. Very recently, Poole and colleagues have proposed a relationship between the CydDC transporter and the periplasmic nickel and heme binding protein NikA (*72*).

Second, the irreversibility of heme reduction suggests that the oxidation state change of the heme is coupled to another change in structure or conformation. One possibility is oxidation and reduction of a disulfide bridge in the protein. Three-dimensional sequence alignment with the related cobalamin transport protein BtuF (*48*, *49*) indicates that C47 and C58 in SiaA are in position to make a disulfide bond. The reactivity of some heme proteins has been shown to be controlled by a dithiol/disulfide interconversion (*73*−*75*). In particular, there is precedence for this interconversion affecting binding to the heme in neuroglobin and cytoglobin (*76*−*78*). Beyond this, there is speculation about a role of the dithiol/disulfide interconversion in metal uptake via ABC transporters, but only limited experimental evidence exists to date (*79*, *80*).

*Denaturation*. In general, heme proteins with Met-His ligands are more stable in the ferrous form. This is true for SiaA, which has midpoints for guanidinium-induced unfolding of 3.1 ± 0.1 M for the oxidized and 5.0 ± 0.1 M for the reduced protein. The $\Delta G(H_2O)$ values for the oxidized and reduced proteins were 7.3 ± 0.8 and 16.0 ± 3.6 kcal mol$^{-1}$, respectively. The difference in the stability between the oxidized and reduced proteins is slightly greater than that for cytochrome $b_{562}$ (4.3 ± 0.5 and 10.3 ± 2.4 kcal mol$^{-1}$, respectively) (*81*) and greater than the difference between the forms of *D. vulgaris* $c_{553}$ (9.1 ± 0.5 and 10.8 ± 0.7 kcal mol$^{-1}$, respectively) (*66*). The $\Delta G(H_2O)$ is slightly less than the differences for horse cytochrome *c* (9.6 ± 0.3 and 17.7 ± 0.7 kcal mol$^{-1}$, respectively) and yeast cytochrome *c* (5.7 ± 0.2 and 15.1 ± 0.7 kcal mol$^{-1}$, respectively) (*82*). In all of these examples with Met-His ligation, the ferric form is less stable than the ferrous form.

The *m* values express the dependence of $\Delta G(H_2O)$ on the concentration of denaturant. In general, they are thought to correlate with the solvent-accessible surface area of the protein upon unfolding (*83*). The values for SiaA are similar to those of horse (104 residues) and yeast (108 residues) cytochrome *c* (*82*) and *D. vulgaris* $c_{553}$ (79 residues) (*66*), although SiaA is a considerably larger protein (282 residues). The fact that the heme is covalently attached to these cytochromes, but not to SiaA, may affect the *m* values. The *m* values of the oxidized and reduced forms of SiaA are similar to one another, as expected because the two forms of the protein are essentially the same size; this was found previously for the cytochromes above.

Comparison of protein unfolding in the two oxidation states with rate constants for heme/hemin transfer can provide insight into the extent to which specific protein−protein interactions are important in this transfer. The rate constants for heme/hemin transfer from Shp to SiaA (HtsA) have been measured by Nygaard et al. (*17*). FerroShp transfers its heme to apoSiaA with a rate constant of 28 ± 6 s$^{-1}$; transfer of the oxidized heme from ferriShp is less than 2-fold faster (43 ± 3 s$^{-1}$). For both oxidation states, the heme transfer is affinity-driven. The rate of transfer from the ferric protein is faster than that from the ferrous protein, consistent with the unfolding data. However, the rates in the two oxidation states are similar to one another, whereas the free energies of unfolding differ noticeably. This is consistent with the importance of protein−protein interactions in determining the rate of heme transfer between these two proteins.

*Homologous Heme Proteins with Different Axial Ligands.* Herein, we have shown that SiaA from the Gram positive *S. pyogenes* has methionine and histidine axial ligands. This is also the case for the homologous protein IsdE from *S. aureus* (*8*, *10*). In contrast, ShuT, from the Gram negative *S. dysenteriae*, has a single tyrosine as an axial ligand (*7*). There is at least one other known example of a heme protein with different sets of axial ligands in two different organisms, the CO-sensing transcriptional activator, CooA (*84*−*88*). Overall, however, the phenomenon is rare. Different sets of axial ligands in the heme binding protein in ABC transporters argue for subtleties in heme uptake and release from the partner proteins in the heme transfer pathways. An understanding of these subtleties will be key in evaluating the heme uptake pathway as a target for new therapeutics designed to circumvent the growing antibiotic resistance of pathogenic bacteria (*9*).

## ACKNOWLEDGMENT

D.W.D. thanks Drs. Siming Wang and Sekar Chandrasekaran as well as Sarah Shealy Cepada, Brian Basden, Marianna Libkind, and Michelle Kim for technical assistance. K.R.R. would like to thank Professor Brian Gibney for technical advice with regard to potential measurements and Gudrun Lukat-Rodgers for helpful discussions.

## REFERENCES

1. Griffiths, E., and Williams, P. (1999) The iron-uptake systems of pathogenic bacteria, fungi and protozoa, in *Iron and Infection: Molecular, Physiological and Clinical Aspects* (Bullen, J. J., Griffiths, E., and Bullen, D. J., Eds.) pp 87−212, John Wiley, Chichester, U.K.
2. Jones, P. M., and George, A. M. (2004) The ABC transporter structure and mechanism: Perspectives on recent research, *Cell Mol. Life Sci. 61*, 682−699.
3. Davidson, A. L., and Chen, J. (2004) ATP-binding cassette transporters in bacteria, *Annu. Rev. Biochem. 73*, 241−268.
4. Brown, J. S., and Holden, D. W. (2002) Iron acquisition by Gram-positive bacterial pathogens, *Microbes Infect. 4*, 1149−1156.
5. Stojiljkovic, I., and Perkins-Balding, D. (2002) Processing of heme and heme-containing proteins by bacteria, *DNA Cell Biol. 21*, 281−295.
6. Crosa, J. H., Mey, A. R., and Payne, S. M. (2004) *Iron Transport in Bacteria*, ASM Press, Washington, DC.
7. Eakanunkul, S., Lukat-Rodgers, G. S., Sumithran, S., Ghosh, A., Rodgers, K. R., Dawson, J. H., and Wilks, A. (2005) Characterization of the periplasmic heme-binding protein ShuT from the heme uptake system of *Shigella dysenteriae*, *Biochemistry 44*, 13179−13191.
8. Mack, J., Vermeiren, C., Heinrichs, D. E., and Stillman, M. J. (2004) *In vivo* heme scavenging by *Staphylococcus aureus* IsdC and IsdE proteins, *Biochem. Biophys. Res. Commun. 320*, 781−788.
9. Maresso, A. W., and Schneewind, O. (2006) Iron acquisition and transport in *Staphylococcus aureus*, *Biometals 19*, 193−203.
10. Grigg, J. C., Vermeiren, C. L., Heinrichs, D. E., and Murphy, M. E. (2007) Heme coordination by *Staphylococcus aureus* IsdE, *J. Biol. Chem., 282*, 28815−28822.
11. Cunningham, M. W. (2000) Pathogenesis of group A streptococcal infections, *Clin. Microbiol. Rev. 13*, 470−511.
12. Francis, R. T., Jr., Booth, J. W., and Becker, R. R. (1985) Uptake of iron from hemoglobin and the haptoglobin-hemoglobin complex by hemolytic bacteria, *Int. J. Biochem. 17*, 767−773.
13. Eichenbaum, Z., Muller, E., Morse, S. A., and Scott, J. R. (1996) Acquisition of iron from host proteins by the group A *Streptococcus*, *Infect. Immun. 64*, 5428−5429.
14. Bates, C. S., Montañez, G. E., Woods, C. R., Vincent, R. M., and Eichenbaum, Z. (2003) Identification and characterization of a *Streptococcus pyogenes* operon involved in binding of hemoproteins and acquisition of iron, *Infect. Immun. 71*, 1042−1055.
15. Lei, B. F., Liu, M. Y., Prater, C. I., Kala, S. V., Deleo, F. R., and Musser, J. M. (2003) Identification and characterization of HtsA, a second heme-binding protein made by *Streptococcus pyogenes*, *Infect. Immun. 71*, 5962−5969.
16. Liu, M. Y., and Lei, B. F. (2005) Heme transfer from streptococcal cell surface protein Shp to HtsA of transporter HtsABC, *Infect. Immun. 73*, 5086−5092.
17. Nygaard, T. K., Blouin, G. C., Liu, M. Y., Fukumura, M., Olson, J. S., Fabian, M., Dooley, D. M., and Lei, B. F. (2006) The mechanism of direct heme transfer from the streptococcal cell surface protein Shp to HtsA of the HtsABC transporter, *J. Biol. Chem. 281*, 20761−20771.
18. Guzman, L. M., Belin, D., Carson, M. J., and Beckwith, J. (1995) Tight regulation, modulation, and high-level expression by vectors containing the arabinose PBAD promoter, *J. Bacteriol. 177*, 4121−4130.
19. Dutton, P. L. (1978) Redox potentiometry: Determination of midpoint potentials of oxidation-reduction components of biological electron-transfer systems, *Methods Enzymol. 54*, 411−435.
20. Huff, A. M., Chang, C. K., Cooper, D. K., Smith, K. M., and Dawson, J. H. (1993) Imidazole-ligated and alkylamine-ligated iron(II, III) chlorin complexes as models for histidine and lysine coordination to iron in dihydroporphyrin-containing proteins: characterization with magnetic circular-dichroism spectroscopy, *Inorg. Chem. 32*, 1460−1466.
21. Bracete, A. M., Sono, M., and Dawson, J. H. (1991) Effects of cyanogen bromide modification of the distal histidine on the spectroscopic and ligand-binding properties of myoglobin: Magnetic circular dichroism spectroscopy as a probe of distal water ligation in ferric high-spin histidine-bound heme proteins, *Biochim. Biophys. Acta 1080*, 264−270.
22. Pond, A. E., Roach, M. P., Thomas, M. R., Boxer, S. G., and Dawson, J. H. (2000) The H93G myoglobin cavity mutant as a versatile template for modeling heme proteins: Ferrous, ferric, and ferryl mixed-ligand complexes with imidazole in the cavity, *Inorg. Chem. 39*, 6061−6066.
23. Pace, C. N., and Scholtz, J. M. (1997) Measuring the Conformational Stability of a Protein, in *Protein Structure: A Practical Approach* (Creighton, T., Ed.) pp 299−321, Oxford University Press, Oxford, U.K.
24. Light, A., and Janska, H. (1989) Enterokinase (enteropeptidase): Comparative aspects, *Trends Biochem. Sci. 14*, 110−112.
25. Kaufmann, R. (1995) Matrix-assisted laser desorption ionization (MALDI) mass spectrometry: A novel analytical tool in molecular biology and biotechnology, *J. Biotechnol. 41*, 155−175.
26. Zhang, W., Niu, S., and Chait, B. T. (1998) Exploring infrared wavelength matrix-assisted laser desorption/ionization of proteins with delayed-extraction time-of-flight mass spectrometry, *J. Am. Soc. Mass Spectrom. 9*, 879−884.
27. Rotsaert, F. A. J., Hallberg, B. M., de Vries, S., Moenne-Loccoz, P., Divne, C., Renganathan, V., and Gold, M. H. (2003) Biophysical and structural analysis of a novel heme *b* iron ligation in the flavocytochrome cellobiose dehydrogenase, *J. Biol. Chem. 278*, 33224−33231.
28. Gonzalez, G., Dioum, E. M., Bertolucci, C. M., Tomita, T., Ikeda-Saito, M., Cheesman, M. R., Watmough, N. J., and Gilles-Gonzalez, M. A. (2002) Nature of the displaceable heme-axial residue in the *Ec*Dos protein, a heme-based sensor from *Escherichia coli*, *Biochemistry 41*, 8414−8421.
29. Cohen, J. D., Bao, W. J., Renganathan, V., Subramaniam, S. S., and Loehr, T. M. (1997) Resonance Raman spectroscopic studies of cellobiose dehydrogenase from *Phanerochaete chrysosporium*, *Arch. Biochem. Biophys. 341*, 321−328.
30. Moore, G. R., Williams, R. J. P., Peterson, J., Thomson, A. J., and Mathews, F. S. (1985) A spectroscopic investigation of the structure and redox properties of *Escherichia coli* cytochrome $b_{562}$, *Biochim. Biophys. Acta 829*, 83−96.
31. Myer, Y. P., and Bullock, P. A. (1978) Cytochrome $b_{562}$ from *Escherichia coli*: Conformational, configurational, and spin-state characterization, *Biochemistry 17*, 3723−3729.
32. Gadsby, P. M. A., and Thomson, A. J. (1990) Assignment of the axial ligands of ferric ion in low-spin hemoproteins by near-infrared magnetic circular-dichroism and electron paramagnetic resonance spectroscopy, *J. Am. Chem. Soc. 112*, 5003−5011.
33. Dawson, J. H., Kadkhodayan, S., Zhuang, C., and Sono, M. (1992) On the use of iron octa-alkylporphyrins as models for protoporphyrin IX-containing heme systems in studies employing magnetic circular dichroism spectroscopy, *J. Inorg. Biochem. 45*, 179−192.

34. Fedurco, M., Augustynski, J., Indiani, C., Smulevich, G., Antalik, M., Bano, M., Sedlak, E., Glascock, M. C., and Dawson, J. H. (2004) The heme iron coordination of unfolded ferric and ferrous cytochrome *c* in neutral and acidic urea solutions. Spectroscopic and electrochemical studies, *Biochim. Biophys. Acta 1703*, 31−41.
35. Perera, R., and Dawson, J. H. (2004) Modeling heme protein active sites with the His93Gly cavity mutant of sperm whale myoglobin: Complexes with nitrogen-, oxygen- and sulfur-donor proximal ligands, *J. Porphyrins Phthalocyanines 8*, 246−254.
36. Durley, R. C. E., and Mathews, F. S. (1996) Refinement and structural analysis of bovine cytochrome $b_5$ at 1.5 Å resolution, *Acta Crystallogr., Sect. D 52*, 65−76.
37. Cheek, J., Mandelman, D., Poulos, T. L., and Dawson, J. H. (1999) A study of the K(+)-site mutant of ascorbate peroxidase: Mutations of protein residues on the proximal side of the heme cause changes in iron ligation on the distal side, *J. Biol. Inorg. Chem. 4*, 64−72.
38. Wand, A. J., Di Stefano, D. L., Feng, Y., Roder, H., and Englander, S. W. (1989) Proton resonance assignments of horse ferrocytochrome *c*, *Biochemistry 28*, 186−194.
39. Gao, Y., Boyd, J., Williams, R. J. P., and Pielak, G. J. (1990) Assignment of proton resonances, identification of secondary structural elements, and analysis of backbone chemical shifts for the C102T variant of yeast iso-1-cytochrome *c* and horse cytochrome *c*, *Biochemistry 29*, 6994−7003.
40. Chau, M.-H., Cai, M. L., and Timkovich, R. (1990) NMR comparison of prokaryotic and eukaryotic cytochromes *c*, *Biochemistry 29*, 5076−5087.
41. Detlefsen, D. J., Thanabal, V., Pecoraro, V. L., and Wagner, G. (1990) Sequential $^1$H NMR assignments of iron(II) cytochrome $c_{551}$ from *Pseudomonas aeruginosa*, *Biochemistry 29*, 9377−9386.
42. Cai, M. L., and Timkovich, R. (1991) Proton resonance assignments for *Pseudomonas aeruginosa* ferrocytochrome $c_{551}$, *Biochem. Biophys. Res. Commun. 178*, 309−314.
43. Cai, M., and Timkovich, R. (1992) Ionization of the heme propionate substituents in pseudomonad cytochromes $c_{551}$, *FEBS Lett. 311*, 213−216.
44. Marion, D., and Guerlesquin, F. (1992) Sequential NMR resonance assignment and secondary structure of ferrocytochrome $c_{553}$ from *Desulfovibrio vulgaris* Hildenborough, *Biochemistry 31*, 8171−8179.
45. Saraiva, L. M., Denariaz, G., Liu, M.-Y., Payne, W. J., Le Gall, J., and Moura, I. (1992) NMR and EPR studies on a monoheme cytochrome $c_{550}$ isolated from *Bacillus halodenitrificans*, *Eur. J. Biochem. 204*, 1131−1139.
46. Barker, P. D., and Freund, S. M. (1996) Bis-methionine ligation to heme iron in mutants of cytochrome $b_{562}$. 2. Characterization by NMR of heme-ligand interactions, *Biochemistry 35*, 13627−13635.
47. Arnesano, F., Banci, L., Bertini, I., Ciofi-Baffoni, S., Woodyear, T. D., Johnson, C. M., and Barker, P. D. (2000) Structural consequences of *b*- to *c*-type heme conversion in oxidized *Escherichia coli* cytochrome $b_{562}$, *Biochemistry 39*, 1499−1514.
48. Borths, E. L., Locher, K. P., Lee, A. T., and Rees, D. C. (2002) The structure of *Escherichia coli* BtuF and binding to its cognate ATP binding cassette transporter, *Proc. Natl. Acad. Sci. U.S.A. 99*, 16642−16647.
49. Locher, K. P., and Borths, E. (2004) ABC transporter architecture and mechanism: Implications from the crystal structures of BtuCD and BtuF, *FEBS Lett. 564*, 264−268.
50. Clarke, T. E., Braun, V., Winkelmann, G., Tari, L. W., and Vogel, H. J. (2002) X-ray crystallographic structures of the *Escherichia coli* periplasmic protein FhuD bound to hydroxamate-type siderophores and the antibiotic albomycin, *J. Biol. Chem. 277*, 13966−13972.
51. Muller, A., Wilkinson, A. J., Wilson, K. S., and Duhme-Klair, A. K. (2006) An $[\{Fe(mecam)\}_2]^{6-}$ bridge in the crystal structure of a ferric enterobactin binding protein, *Angew. Chem., Int. Ed. 45*, 5132−5136.
52. Xavier, A. V., Czerwinski, E. W., Bethge, P. H., and Mathews, F. S. (1978) Identification of the haem ligands of cytochrome $b_{562}$ by X-ray and NMR methods, *Nature 275*, 245−247.
53. Mathews, F. S., Bethge, P. H., and Czerwinski, E. W. (1979) The structure of cytochrome $b_{562}$ from *Escheria coli* at 2.5 Å resolution, *J. Biol. Chem. 254*, 1699−1706.
54. Bullock, P. A., and Myer, Y. P. (1978) Circular dichroism and resonance Raman studies of cytochrome $b_{562}$ from *Escherichia coli*, *Biochemistry 17*, 3084−3091.
55. Bogumil, R., Maurus, R., Hildebrand, D. P., Brayer, G. D., and Mauk, A. G. (1995) Origin of the pH-dependent spectroscopic properties of pentacoordinate metmyoglobin variants, *Biochemistry 34*, 10483−10490.
56. Gadsby, P. M. A., and Thomson, A. J. (1982) Identification of the imidazolate anion as a ligand in metmyoglobin by near infrared magnetic circular dichroism spectroscopy, *FEBS Lett. 150*, 59−63.
57. Banci, L., Bertini, I., Turano, P., and Oliver, M. V. (1992) NOE and two-dimensional correlated $^1$H-NMR spectroscopy of cytochrome *c*′ from *Chromatium vinosum*, *Eur. J. Biochem. 204*, 107−112.
58. La Mar, G. N., Jackson, J. T., Dugad, L. B., Cusanovich, M. A., and Bartsch, R. G. (1990) Proton NMR study of the comparative electronic/magnetic properties and dynamics of the acid ↔ alkaline transition in a series of ferricytochromes *c*′, *J. Biol. Chem. 265*, 16173−16180.
59. Dolla, A., Blanchard, L., Guerlesquin, F., and Bruschi, M. (1994) The protein moiety modulates the redox potential in cytochromes *c*, *Biochimie 76*, 471−479.
60. Mauk, A. G., and Moore, G. R. (1997) Control of metalloprotein redox potentials: what does site-directed mutagenesis of hemoproteins tell us? *J. Biol. Inorg. Chem. 2*, 119−125.
61. Springs, S. L., Bass, S. E., and McLendon, G. L. (2000) Cytochrome $b_{562}$ variants: A library for examining redox potential evolution, *Biochemistry 39*, 6075−6082.
62. Springs, S. L., Bass, S. E., Bowman, G., Nodelman, I., Schutt, C. E., and McLendon, G. L. (2002) A multigeneration analysis of cytochrome $b_{562}$ redox variants: Evolutionary strategies for modulating redox potential revealed using a library approach, *Biochemistry 41*, 4321−4328.
63. Igarashi, K., Verhagen, M. F. J. M., Samejima, M., Schulein, M., Eriksson, K. E. L., and Nishino, T. (1999) Cellobiose dehydrogenase from the fungi *Phanerochaete chrysosporium* and *Humicola insolens*: A flavohemoprotein from *Humicola insolens* contains 6-hydroxy-FAD as the dominant active cofactor, *J. Biol. Chem. 274*, 3338−3344.
64. Mao, J. J., Hauser, K., and Gunner, M. R. (2003) How cytochromes with different folds control heme redox potentials, *Biochemistry 42*, 9829−9840.
65. Goto, T., Matsuno, T., Hishinuma-Narisawa, M., Yamazaki, K., Matsuyama, H., Inoue, N., and Yumoto, I. (2005) Cytochrome *c* and bioenergetic hypothetical model for alkaliphilic *Bacillus* spp, *J. Biosci. Bioeng. 100*, 365−379.
66. Wittung-Stafshede, P. (1999) Equilibrium unfolding of a small low-potential cytochrome, cytochrome $c_{553}$ from *Desulfovibrio vulgaris*, *Protein Sci. 8*, 1523−1529.
67. Benini, S., Borsari, M., Ciurli, S., Dikiy, A., and Lamborghini, M. (1998) Modulation of *Bacillus pasteurii* cytochrome $c_{553}$ reduction potential by structural and solution parameters, *J. Biol. Inorg. Chem. 3*, 371−382.
68. Izadi, N., Henry, Y., Haladjian, J., Goldberg, M. E., Wandersman, C., Delepierre, M., and Lecroisey, A. (1997) Purification and characterization of an extracellular heme-binding protein, HasA, involved in heme iron acquisition, *Biochemistry 36*, 7050−7057.
69. Block, D. R., and Rodgers, K. R. (2007) Unpublished experiments.
70. Pittman, M. S., Corker, H., Wu, G., Binet, M. B., Moir, A. J., and Poole, R. K. (2002) Cysteine is exported from the *Escherichia coli* cytoplasm by CydDC, an ATP-binding cassette-type transporter required for cytochrome assembly, *J. Biol. Chem. 277*, 49841−49849.
71. Pittman, M. S., Robinson, H. C., and Poole, R. K. (2005) A bacterial glutathione transporter (*Escherichia coli* CydDC) exports reductant to the periplasm, *J. Biol. Chem. 280*, 32254−32261.
72. Shepherd, M., Heath, M. D., and Poole, R. K. (2007) NikA binds heme: A new role for an *Escherichia coli* periplasmic nickel-binding protein, *Biochemistry 46*, 5030−5037.
73. Osyczka, A., Dutton, P. L., Moser, C. C., Darrouzet, E., and Daldal, F. (2001) Controlling the functionality of cytochrome $c_1$ redox potentials in the *Rhodobacter capsulatus* $bc_1$ complex through disulfide anchoring of a loop and a beta-branched amino acid near the heme-ligating methionine, *Biochemistry 40*, 14547−14556.
74. Storch, E. M., Daggett, V., and Atkins, W. M. (1999) Engineering out motion: Introduction of a *de novo* disulfide bond and a salt bridge designed to close a dynamic cleft on the surface of cytochrome $b_5$, *Biochemistry 20*, 5054−5064.

75. Storch, E. M., Grinstead, J. S., Campbell, A. P., Daggett, V., and Atkins, W. M. (1999) Engineering out motion: A surface disulfide bond alters the mobility of tryptophan 22 in cytochrome $b_5$ as probed by time-resolved fluorescence and $^1$H NMR experiments, *Biochemistry 20*, 5065−5075.
76. Hamdane, D., Kiger, L., Dewilde, S., Green, B. N., Pesce, A., Uzan, J., Burmester, T., Hankeln, T., Bolognesi, M., Moens, L., and Marden, M. C. (2003) The redox state of the cell regulates the ligand binding affinity of human neuroglobin and cytoglobin, *J. Biol. Chem. 278*, 51713−51721.
77. Hamdane, D., Kiger, L., Dewilde, S., Uzan, J., Burmester, T., Hankeln, T., Moens, L., and Marden, M. C. (2005) Hyperthermal stability of neuroglobin and cytoglobin, *FEBS J. 272*, 2076−2084.
78. Hankeln, T., Ebner, B., Fuchs, C., Gerlach, F., Haberkamp, M., Laufs, T. L., Roesner, A., Schmidt, M., Weich, B., Wystub, S., Saaler-Reinhardt, S., Reuss, S., Bolognesi, M., De Sanctis, D., Marden, M. C., Kiger, L., Moens, L., Dewilde, S., Nevo, E., Avivi, A., Weber, R. E., Fago, A., and Burmester, T. (2005) Neuroglobin and cytoglobin in search of their role in the vertebrate globin family, *J. Inorg. Biochem. 99*, 110−119.
79. Rukhman, V., Anati, R., Melamed-Frank, M., and Adir, N. (2005) The MntC crystal structure suggests that import of $Mn^{2+}$ in cyanobacteria is redox controlled, *J. Mol. Biol. 348*, 961−969.
80. Chandra, B. R., Yogavel, M., and Sharma, A. (2007) Structural analysis of ABC-family periplasmic zinc binding protein provides new insights into mechanism of ligand uptake and release, *J. Mol. Biol. 367*, 970−982.
81. Wittung-Stafshede, P., Lee, J. C., Winkler, J. R., and Gray, H. B. (1999) Cytochrome $b_{562}$ folding triggered by electron transfer: Approaching the speed limit for formation of a four-helix-bundle protein, *Proc. Natl. Acad. Sci. U.S.A. 96*, 6587−6590.
82. Mines, G. A., Pascher, T., Lee, S. C., Winkler, J. R., and Gray, H. B. (1996) Cytochrome *c* folding triggered by electron transfer, *Chem. Biol. 3*, 491−497.
83. Myers, J. K., Pace, C. N., and Scholtz, J. M. (1995) Denaturant *m* values and heat capacity changes: Relation to changes in accessible surface areas of protein unfolding, *Protein Sci. 4*, 2138−2148.
84. Roberts, G. P., Thorsteinsson, M. V., Kerby, R. L., Lanzilotta, W. N., and Poulos, T. (2001) CooA: A heme-containing regulatory protein that serves as a specific sensor of both carbon monoxide and redox state, *Prog. Nucleic Acid Res. Mol. Biol. 67*, 35−63.
85. Yamashita, T., Hoashi, Y., Watanabe, K., Tomisugi, Y., Ishikawa, Y., and Uno, T. (2004) Roles of heme axial ligands in the regulation of CO binding to CooA, *J. Biol. Chem. 279*, 21394−21400.
86. Clark, R. W., Youn, H., Lee, A. J., Roberts, G. P., and Burstyn, J. N. (2007) DNA binding by an imidazole-sensing CooA variant is dependent on the heme redox state, *J. Biol. Inorg. Chem. 12*, 139−146.
87. Inagaki, S., Masuda, C., Akaishi, T., Nakajima, H., Yoshioka, S., Ohta, T., Pal, B., Kitagawa, T., and Aono, S. (2005) Spectroscopic and redox properties of a CooA homologue from *Carboxydothermus hydrogenoformans*, *J. Biol. Chem. 280*, 3269−3274.
88. Komori, H., Inagaki, S., Yoshioka, S., Aono, S., and Higuchi, Y. (2007) Crystal structure of CO-sensing transcription activator CooA bound to exogenous ligand imidazole, *J. Mol. Biol. 367*, 864−871.

BI701604Y